Sensors and Actuators B 261 (2018) 1–10

Contents lists available at ScienceDirect

Sensors and Actuators B: Chemical

journal homepage: www.elsevier.com/locate/snb

A novel natural surface-enhanced Raman spectroscopy (SERS) substrate based on graphene oxide-Ag nanoparticles-Mytilus coruscus hybrid system

Zhengyi Lu[a], Yanjun Liu[b,*], Minghong Wang[a], Chao Zhang[a], Zhen Li[a], Yanyan Huo[a], Zhe Li[a], Shicai Xu[c], Baoyuan Man[a], Shouzhen Jiang[a,d,**]

[a] School of Physics and Electronics, Shandong Normal University, Jinan 250014, China
[b] Department of Electrical and Electronic Engineering, Southern University of Science and Technology, Shenzhen 518055, China
[c] Shandong Provincial Key Laboratory of Biophysics, College of Physics and Electronic Information, Dezhou University, Dezhou 253023, China
[d] Shandong Provincial Key Laboratory of Optics and Photonic Device, Jinan 250014, China

ARTICLE INFO

Article history:
Received 25 October 2017
Received in revised form 11 January 2018
Accepted 11 January 2018
Available online 12 January 2018

Keywords:
SERS
Mytilus coruscus
Graphene oxide
Reproducibility
Stability

ABSTRACT

Recently, biological materials have attracted more and more attentions on preparing the surface-enhanced Raman spectroscopy (SERS) substrate with the conspicuous SERS performance. Herein, we demonstrate a simply facile and inexpensive approach to fabricate a novel natural SERS substrate based on graphene oxide-Ag nanoparticles-Mytilus coruscus (GO-AgNPs-M.c.). The surface-enhanced resonance Raman spectroscopy (SERRS) signals of the Rhodamine 6G (R6G) on the GO-AgNPs-M.c. hybrids exhibit the much better SERRS performances in terms of the sensitivity, the signal reproducibility and the antioxidant stability than that on the AgNPs-M.c. one. The well electric field enhancement contribution is likewise confirmed in theory via the COMSOL software. Moreover, the successful detection of trace malachite green (MG) and methylene blue (MB) indicates the well feasibility for multi-molecules detection on the GO-AgNPs-M.c. hybrids. Thus, this inexpensive and high-efficiency natural SERS substrate have great potential for the considerable biochemical SERS applications and broaden the way for preparing multiple SERS platforms derived from other natural materials.

1. Introduction

Surfaced enhanced Raman spectroscopy (SERS), as a versatile analytical technique which could provide single molecular sensitivity, has attracted increasing attentions of both theoretical and experimental researchers in recent decades [1–4]. Due to the ultra-sensitive and label-free detection of chemical and biological molecules, SERS has shown great potential for practical applications in diverse fields, such as environmental monitoring, food safety, biomedical diagnostics, gas sensors and explosives in military [5–10]. It is generally accepted that electromagnetic mechanism (EM) and chemical mechanism (CM) are the major mechanisms of SERS enhancement [7,11]. The EM, originating from the dramatic increase of local electromagnetic field in the plasmonic "hot spots" supported by strong coupling of localized surface plasmon resonance (LSPR), can provide a far higher enhancement factor than the CM which results from the charge transfer between the probing molecules and the substrate [12–14]. It is commonly believed that the noble metal with hybrid plasmonic structures can offer a prominent SERS effect from the EM. Thence, the efficient plasmonic nanostructures or configurations have been designed to achieve the highly sensitive SERS detection of trace molecules [11,15]. Diverse technologies (such as lithography techniques, nanosphere masks, self-assembly, porous silicon template etc.) have been emerging for developing the SERS substrate with the homogeneous plasmonic arrays [16–21]. However, the facile and inexpensive preparation of the meaningful SERS substrate with uniformly well-ordered arrays remains to be a significant challenge.

Recently, systematic studies have confirmed that certain biological materials possess the unique structural properties which could be applied in the material science [22,23]. In terms of the fascinating micro/nanostructures and the low-cost acquirement of the biological materials, the novel natural SERS substrates have been emerging endlessly [24–28]. Considerable research efforts have been investi-

* Corresponding author at: Department of Electrical and Electronic Engineering, Southern University of Science and Technology, Shenzhen 518055, China.
** Corresponding author at: School of Physics and Electronics, Shandong Normal University, Jinan 250014, China.
E-mail addresses: yjliu@sustc.edu.cn (Y. Liu), jiang_sz@126.com (S. Jiang).

https://doi.org/10.1016/j.snb.2018.01.113
0925-4005/

gated that these biological templates simply decorated with the plasmonic metals could show the conspicuous SERS effect for multi-molecules detection. For example, Mu and co-workers in situ synthesized gold nanoparticles on the surface of several butterfly wings with natural photonic architectures, achieving the detection of 10^{-9} M 4-aminothiophenol (4-ATP) [24]. According to Shao's work, the novel platform with hierarchical nanogaps was designed by performing the cicada wings as bioscaffold arrays and successfully applied in the animal virus biosensing [26]. Besides, Huang and colleagues fabricated the natural substrate based on silver deposited taro leaf, which obtained highly sensitive and well reproducible signals by means of natural superhydrophobicity and rich hot spots provided by crossed nanoplate [27]. While these works achieve the well SERS performance based on the natural arrays, several disadvantages remain to exist. First, the poor manipuility of the fabricated natural SERS substrate greatly limits the practical applications. Since these biological materials are fragile, easily damaged during the fabrication process and the experimental measurement. Second, seasonal restriction and biological devastation of natural materials have prevented substrates from being prepared promptly to certain extent. Third, the oxidation of the noble metal (especially sliver) directly decreases the long-term endurance of natural SERS substrates. Therefore, the more suitable natural template still need to be researched for fabricating the SERS substrate achieving the highly sensitive measurements with the excellent reproducibility and the well stability.

Mytilus coruscus (M.c.), belonging to mytilidae, is an extremely common edible aquatic mollusk. The shell of M.c. has been mostly thrown away after eating and become almost useless. Yet, recent research efforts have suggested that the internal surface of the shell exhibits the extremely exciting microstructures and may be divided into three regions: nacre region (N) region, adductor muscle scar (AMS) region and fibrous prism (FP) region [29–31]. More surprisingly, these unique microstructures on the M.c. are most likely to be utilized to prepare the plasmonic structures for the SERS measurement, including several advantages: excellent uniform microstructures in large scale, the high manipuility due to the antifragile property, easily massive obtainment at low cost.

Graphene, as a typical two-dimensional nanomaterial with superior optical and electronic properties, has been increasingly applied to the SERS substrate, since it can further enlarge the SERS signals on account of the CM and suppress the fluorescence background from the probing molecules [32–35]. Compared to graphene, graphene oxide (GO) has rich oxygen-containing groups, which are more critical for the selective adsorption of molecules and the achievement of the SERS signals with well homogeneity, chemical stability and bio-compatibility [36–38]. Moreover, the GO can be used as the additional protective layer to maintain the stability of the SERS substrate [39].

In this paper, by combining the above advantages, we reported a novel natural SERS substrate based on graphene oxide-Ag nanoparticles-Mytilus coruscus (GO-AgNPs-M.c.). With R6G as the analyte molecules, the SERRS behavior of the three regions (N, AMS and FP) was firstly analysed on the non-decorated AgNPs-M.c. substrate. The FP region exhibited the best SERRS behavior due to abundant hot spots around the three-dimension (3D) active plasmonic natural structures. Furthermore, the GO-AgNPs-M.c. hybrids were fabricated by dip-coating the GO film on the AgNPs-M.c. hybrids, which achieved the more sensitive, reproducible and stable SERRS signals compared with the non-decorated AgNPs-M.c. hybrids. The minimum detectable concentration for R6G on the GO-AgNPs-M.c. substrate can reach 10^{-14} M. The well electric field enhancement distribution is further confirmed by the COMSOL software. Experimental results demonstrate that the well-ordered natural arrays and the homogeneous decoration of GO lead to the excellent reproducibility and the well antioxidant stability of SERRS signals. What's more, the successful detection of malachite green (MG) and methylene blue (MB) indicates that the GO-AgNPs-M.c. hybrids show the immerse potential for practical applications in diverse biochemical fields.

2. Experimental

2.1. Preparation of the AgNPs-M.c. and GO-AgNPs-M.c. substrates

Fig. 1 schematically illustrates the fabrication processes of the AgNPs-M.c. and GO-AgNPs-M.c. substrates. The M.c. was collected from Rizhao, located at the seaside of Huanghai Sea in China. The length of selected shell for the experiment is approximately 6 cm. After the remove of the whole soft tissue by a knife, the shell was firstly treated with the alkali dissolution method, i.e. immersing the shell into the NaOH aqueous solution (20%, w/v) under the water bath 65 °C for 1 h to remove the organic contaminants adhered to M.c. and eliminate the cuticle and partial organic membrane. The shell was subsequently put into Deionized water bath sonication for 10 min twice, then dried in the N_2 atmosphere. Afterwards, 0.001 g silver wire was deposited on the M.c. by the physical vapor deposition (PVD) method, forming the AgNPs-M.c. substrate. Furthermore, the 20 μL GO suspension with the concentration of 0.2 mg/mL was dip-coated on the AgNPs-M.c. substrate, fabricating the GO-AgNPs-M.c. substrate. The prepared AgNPs-M.c. and GO-AgNPs-M.c. substrates were sealed in the vacuum environment for the following SERS measurements. What needs illustration is that we merely deposited AgNPs at the whole M.c. surface in order to compare the surface morphology and the SERS performance of three regions. With respect to all other measurements, only FP region was separated from the M.c. by a knife to fabricate the AgNPs-M.c. and GO-AgNPs-M.c. substrates.

2.2. SERS experiments

The R6G solution obtained by dissolving the R6G in the water was used to test and compare the SERRS performances of different regions on the AgNPs-M.c. substrate and different prepared substrates (SiO_2, AgNPs-M.c. and GO-AgNPs-M.c.). The malachite green (MG) and methylene blue (MB) from 10^{-5} to 10^{-9} M were also used to detect the SERS effect of GO-AgNPs-M.c. substrate. 2 μL of these probe molecules solution was dropped directly on the tested substrates. Then, these samples were totally dried before performing the SERS experiments. The mentioned SERS spectra were collected with a Horiba HR Evolution 800 Raman spectrometer system (laser wavelength at 532 nm, 4.8 mW laser power, gratings with 600 grooves per 1 mm, × 50 objective lens, 1 μm laser spot, 8 s acquisition time etc.). These SERS spectra are completely the average of spectra randomly collected from at least 8 points on all substrates.

2.3. Characterization

The surface structures of all the substrates were characterized by scanning electron microscope (SEM, Zeiss Gemini Ultra–55). The energy dispersive spectroscopy (EDS) was utilized for the chemical elemental analysis. All Raman spectra were carried out with a Raman spectrometer (Horiba HR Evolution 800).

3. Results and discussion

As shown in Fig. 1, the image of M.c. can be seen clearly, the blue circle from left to right represents the N, AMS and FP regions, respectively. The surface morphologies of three regions were further investigated by the SEM images. As shown in Fig. 2(a) and (b), the morphology and cross-sectional SEM images of the N region

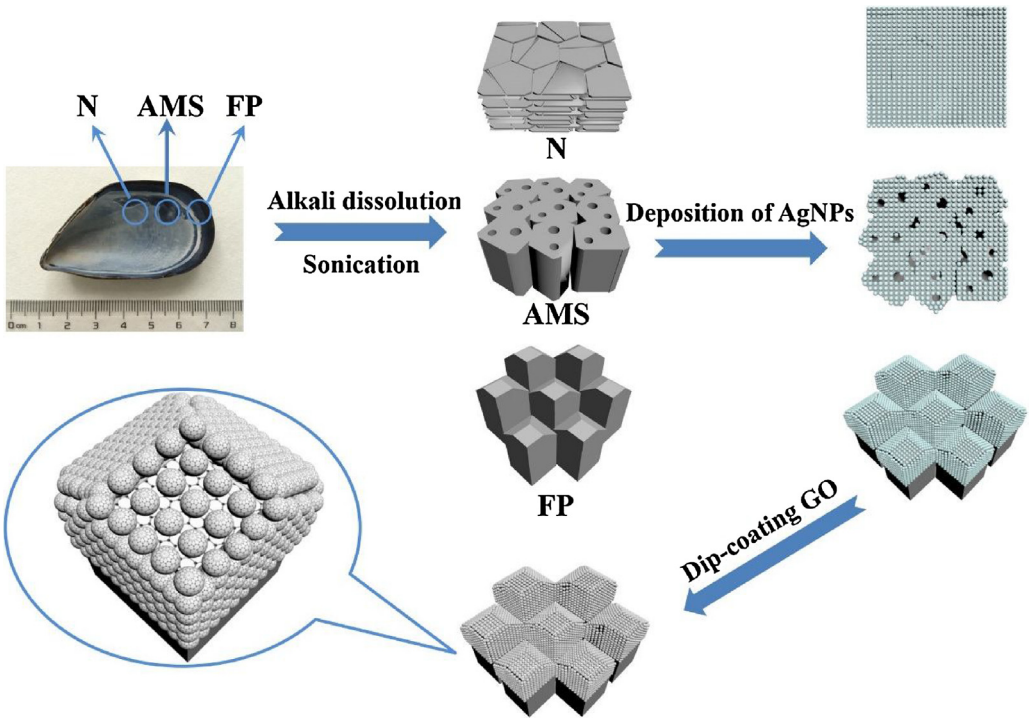

Fig. 1. Preparation processes of the AgNPs-M.c. and GO-AgNPs-M.c. substrates.

prove that the N region consists of the neat lamellar stacking structures. Moreover, the surface topography of the N region displays some cracking flat tablets densely packed together, similar to the turtle shell. The morphology and cross-sectional SEM images of the AMS region are shown in Fig. 2(c) and (d). The myostracums with some narrow silts and voids can be easily observed in the AMS region, and the thickness of AMS region is about 15 μm. Fig. 2(e) exhibits the surface morphology of the FP region, where the highly ordered prisms in a relatively large area can be observed. The inset in Fig. 2(e) indicates that these fibrous prisms are densely stacked. The size of prisms is approximately 1.5 μm at average. These unique structures are beneficial to achieve the well SERS signal, since they can provide much rich hot spots while decorated with the noble metal. The cross-sectional SEM images of the FP region in Fig. 2(f) shows these prisms are entirely distributed in an oblique direction towards the shell margin.

In order to make these natural structures perform as plasmonic platforms, AgNPs were deposited on the M.c. by the PVD method. The SEM images of the N, AMS and FP regions on the AgNPs-M.c. substrate are respectively presented in Fig. 3(a)-(c). As we can see from the insets in Fig. 3(a)-(c), AgNPs has the dense arrangement (narrow nanogap is around 3 nm), and the average size is approximately 20 nm on these natural structures, which was measured with the Nano measurer software. Especially, the AgNPs likewise exist between the prisms densely, which indicates that the well three-dimension (3D) plasmonic structures could have formed. The EDS spectrum in Fig. 3(d) collected from the FP region on the AgNPs-M.c. substrate further confirms that the silver has been successfully deposited on the substrate.

The R6G was chosen as the analyte molecule to evaluate the SERS performance of these three plasmonic structures on the AgNPs-M.c. substrate. When using excitation in 532 nm, we can obtain the SERRS signal of R6G due to the resonance Raman contribution in R6G SERS spectra [40]. The Fig. 3(e) presents the SERRS signals of R6G molecules with the concentration of 10^{-9} M from the three regions. From the typical spectrum collected from FP area on the AgNPs-M.c substrate, the characteristic Raman peaks of R6G at 610, 772, 1182, 1311, 1362, 1506 and 1647 cm^{-1} could be observed clearly [40,41], and the intensity of each Raman bands is much higher than that in other two spectra collected from the AMS and N regions. The obvious bands at 1094 and 1483 cm^{-1} all observed from three regions are assigned to symmetric stretching vibration mode and antisymmetric stretching vibration mode of CO_3^{2-} ions, respectively [29]. The intensity of Raman bands at 1094 and 1483 cm^{-1} for three spectra have some differences, which is highly possible to be caused by the subtle difference for the composition of structures. As shown in Fig. 3(f), the peak intensity of 610 and 772 cm^{-1} were quantitatively compared to estimate the SERRS effect of varied structures on the AgNPs-M.c. substrate. By calculation, the band intensity of 610 cm^{-1} on FP region is approximately 17.5 times stronger than that on N region, 35.7 times higher than that on AMS region. Moreover, the band intensity of 772 cm^{-1} on FP region are approximately 11.6 times stronger than that on N region, 30.6 times higher than that on AMS region. The high Raman enhancement of FP area on the AgNPs-M.c. substrate should be attributed to three major factors. First, AgNPs are densely decorated in the fibrous prisms (especially in the narrow gap between the adjacent prisms), forming 3D plasmonic structures which can provide much abundant hot spots. Second, the effective oscillate of incident laser can occur between the valleys of well-separated prisms, further enhancing the scattering cross-section. Third, the probing molecules could be likely to aggregate in the narrow space between the prisms. Besides, the cracks of NP region and the holes and hollows of AMS region on the AgNPs-M.c. substrate could also produce few hot spots, and the few probing molecule could slightly aggregate in these especial structures, so the low intensity of Raman bands can be still obtained. These results lead us to conclude that the FP region shows the better SERS performance than other regions on the AgNPs-M.c. substrate due to its high-ordered 3D plasmonic structures. Therefore, the substrates for the following measurements were all fabricated by the FP region of M.c..

To continue exploring the SERRS behavior of the FP region, we designed the GO-AgNPs-M.c. substrate. Fig. 4(a) and (b) represent the typical SEM images of the GO-AgNPs-M.c. substrate in

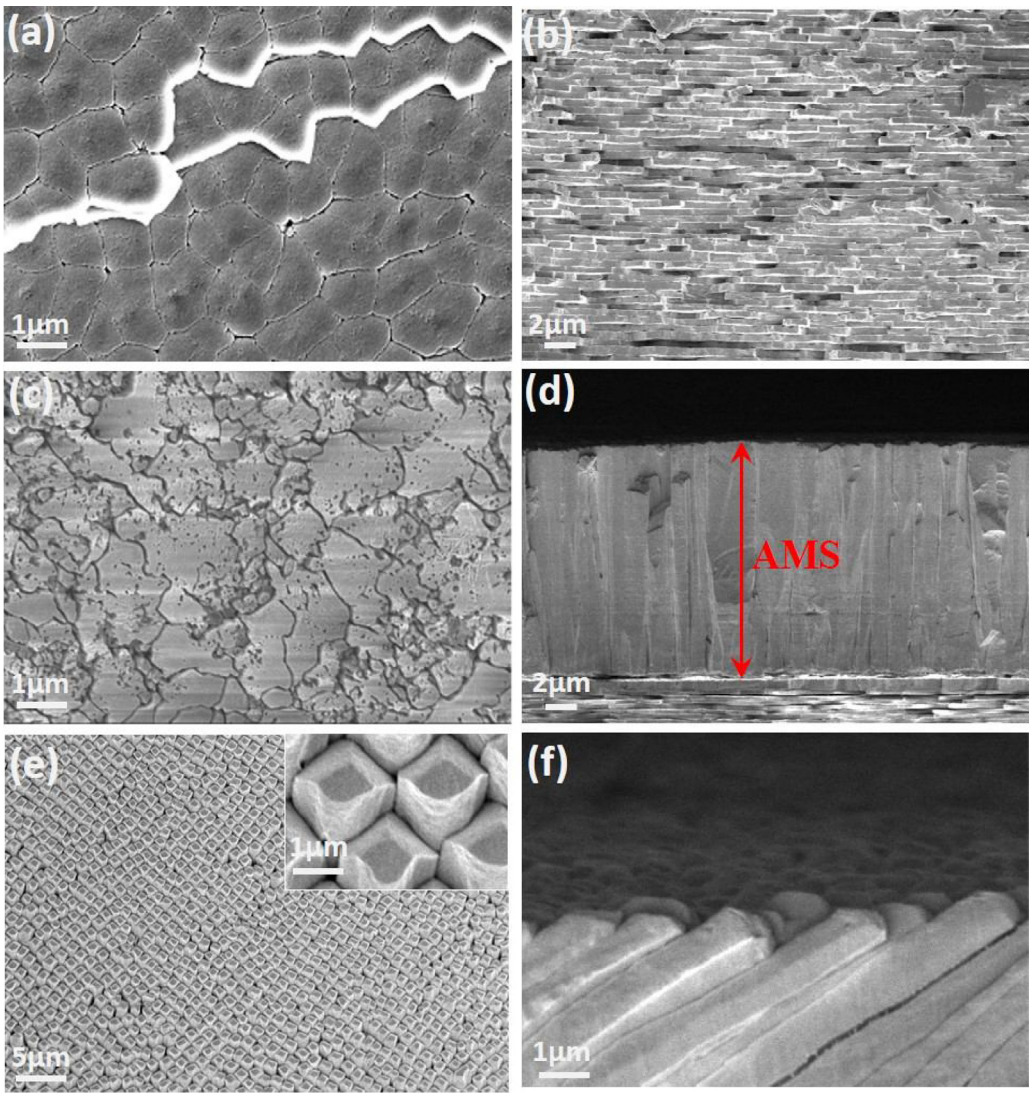

Fig. 2. (a), (c) and (e) represent the typical SEM images of the N, AMS and FP regions on the M.c., respectively. Insert in (e): SEM image of the FP region in a larger magnification. (b), (d) and (f) are the cross-sectional SEM images of the N, AMS and FP regions, respectively.

diverse magnifications. After the decoration of GO, the GO-AgNPs-M.c. substrate still displays typical pyramid-like fibrous prisms. The wrinkles of GO films could be obviously identified between prisms (marked with red arrows), proving that AgNPs-M.c. is covered by the GO film evenly. The origin Raman spectra of the AgNPs-M.c. and GO-AgNPs-M.c. substrates were further measured to confirm the GO decoration, as shown in Fig. 4(a). Apart from the original Raman peaks of AgNPs-M.c. substrate, the GO-AgNPs-M.c. substrate shows two obvious Raman peaks at 1350 and 1587 cm^{-1}, which are related to the D and G bands of the disordered GO, respectively [21,39]. This result further reveals the successful modification of GO on the GO-AgNPs-M.c. substrate. In Fig. 4(d), the Raman mapping of 1350 cm^{-1} peak of GO were obtained over an area of $20 \times 20\ \mu m^2$ on the GO-AgNPs-M.c. substrate. The small color variations of the D peak demonstrated a relatively uniform distribution of GO in large scale.

Fig. 5(a) and (b) illustrate the SERRS signals of R6G with various concentrations on the AgNPs-M.c. and GO-AgNPs-M.c. substrates. All the characteristic vibrations of R6G can be confirmed with the previous mentioned, and the intensity of these bands decay with the decreasing concentrations monotonously. The enhancement effect of the GO-AgNPs-M.c. substrate is clearly superior to the AgNPs-M.c. substrate in term of the intensity of bands. Due to the successful modification of GO, the small bulges of the Raman bands at 1350 and 1585 cm^{-1} appear obvious on the GO-AgNPs-M.c. substrate. Importantly, the detection limit of the GO-AgNPs-M.c. substrate could be down to 10^{-14} M, which is one order of magnitude lower than that of the AgNPs-M.c. substrate. The better SERRS behavior of GO-AgNPs-M.c. hybrids can be ascribed to the following factors: first, the GO can provide the extra enhancement for the SERRS signal from the CM, which is correlated to the charge transfer between the substrate and the target molecules. Second, the GO film could reduce the loss of the target molecules to certain extent. The little partial target molecule solution could inevitably flow into the bottom of prisms along the small gaps between the prisms, inducing the reduction of the effective target molecules, further resulting in the unsatisfactory detections. Third, the AgNPs are closely covered by the GO, so the analyte molecules could be more effectively enriched around the hot spots, further resulting in more sensitive SERRS signals [39].

The relationships between the SERRS intensity of 610 cm^{-1} peak and the concentration of R6G for the GO-AgNPs-M.c. and AgNPs-M.c. substrates are plotted in log scale in Fig. 5(c), where the linear fit curve can be observed. The values of R^2 can reach 0.976 and 0.968 respectively, indicating that these two substrates could provide the quantitative analyze for the concentration of the analyte molecule.

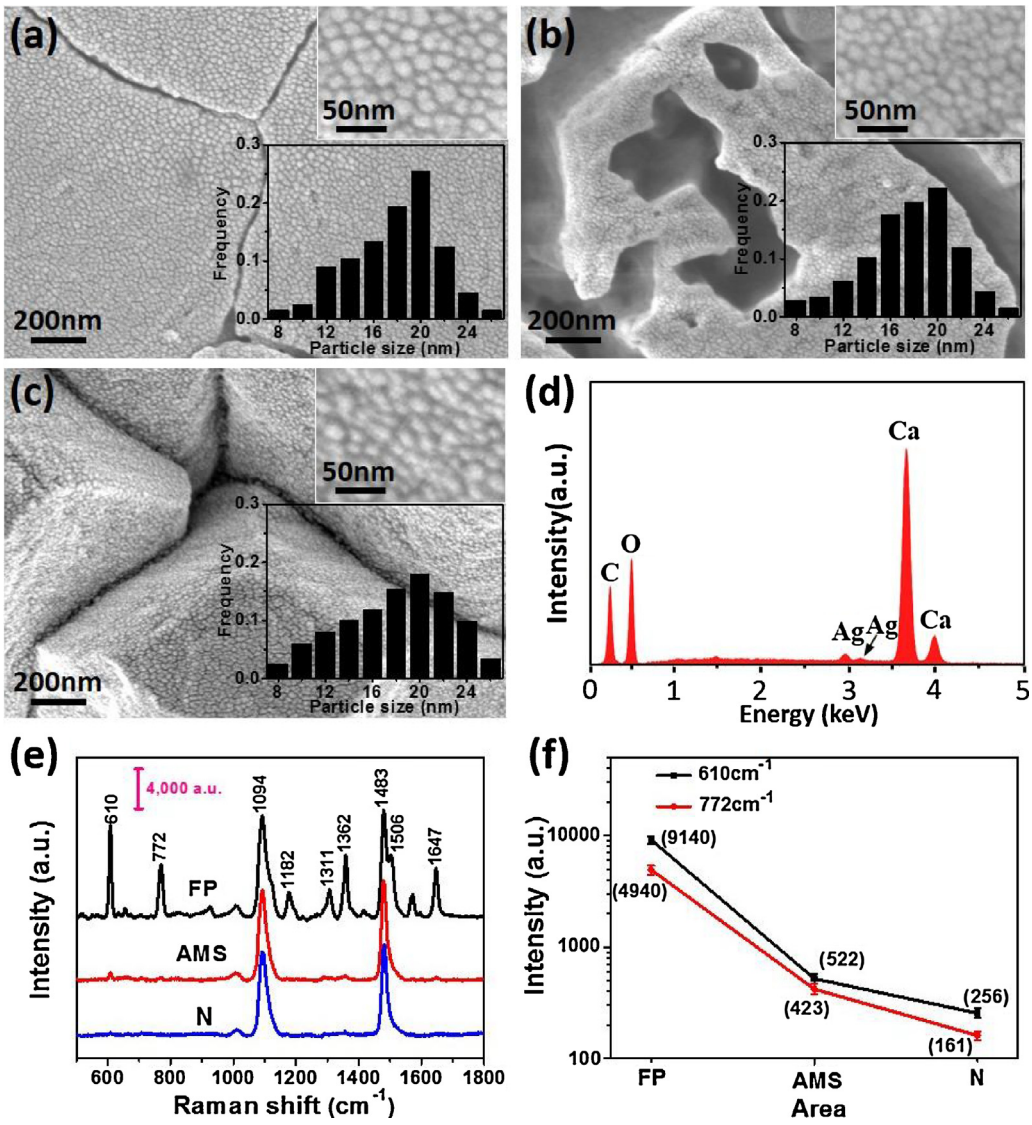

Fig. 3. (a)-(c) are respectively the SEM images of the N, AMS and FP regions on the AgNPs-M.c. substrate. The insets in (a)-(c) are respectively the magnified SEM images and histograms of particle size distribution of the AgNPs. (d) The EDS spectra collected from the FP region on the AgNPs-M.c. substrate. (e) Measured SERRS signals of R6G with the concentration of 10^{-9} M from three regions. (f) The relative SERRS intensity of the peaks at 610 and 772 cm^{-1} in cases of three regions in log scale.

The former R^2 is a bit higher than the latter R^2, attributing to the even distribution of R6G molecules with the existence of GO film on the GO-AgNPs-M.c. substrate.

Fig. 5(d) shows the SERRS signals of 10^{-9} M R6G on the GO-AgNPs-M.c. and AgNPs-M.c. substrates, the resonance Raman signal of 10^{-3} M R6G on blank SiO_2 substrate separately. The enhancement distribution of GO was further quantified by the calculation of the enhancement factor (EF) according to the following formula [25–27,42,43]:

$$EF = \frac{I_{SERS}/N_{SERS}}{I_{RS}/N_{RS}} = \frac{I_{SERS}}{I_{RS}} \times \frac{N_{RS}}{N_{SERS}}$$

where I_{SERS} and I_{RS} represent the peak intensitity of the SERS signal and the normal Raman signal, and N_{SERS} and N_{RS} are the number of molecules on the substrates within the laser spot. The band intensity of 610 cm^{-1} was chosen to calculate the EF. Therefore, the EF for the GO-AgNPs-M.c. hybrids is estimated:

$$\frac{16002\,(a.u.)}{558\,(a.u.)} \times \frac{10^{-3}\,(M)\cdot 2\,(\mu L)\cdot N_A\cdot \left(A_{laser}/A^{dry}_{SiO_2}\right)}{10^{-9}\,(M)\cdot 2\,(\mu L)\cdot N_A\cdot \left(A_{laser}/A^{dry}_{SERS}\right)} \approx 2.4\times 10^7$$

where N_A is Avogadro's constant, $A^{dry}_{SiO_2}$ is the dried area on the SiO_2 substrate, A^{dry}_{SERS} is the dried area on the SERS substrate, A_{laser} is the area of laser spot. The dried area on SiO_2 substrate is approximately 1.2-time larger than that on SERS substrate. Similarly, the EF for the AgNPs-M.c. hybrids is calculated:

$$\frac{7021\,(a.u.)}{558\,(a.u.)} \times \frac{10^{-3}\,(M)\cdot 2\,(\mu L)\cdot N_A\cdot \left(A_{laser}/A^{dry}_{SiO_2}\right)}{10^{-9}\,(M)\cdot 2\,(\mu L)\cdot N_A\cdot \left(A_{laser}/A^{dry}_{SERS}\right)} \approx 1.0\times 10^7$$

Thence, the EF for the GO-AgNPs-M.c. substrate exhibits a 2.4-fold enhancement compared to the AgNPs-M.c. substrate, which agrees with the chemical enhancement caused by the GO layer [38].

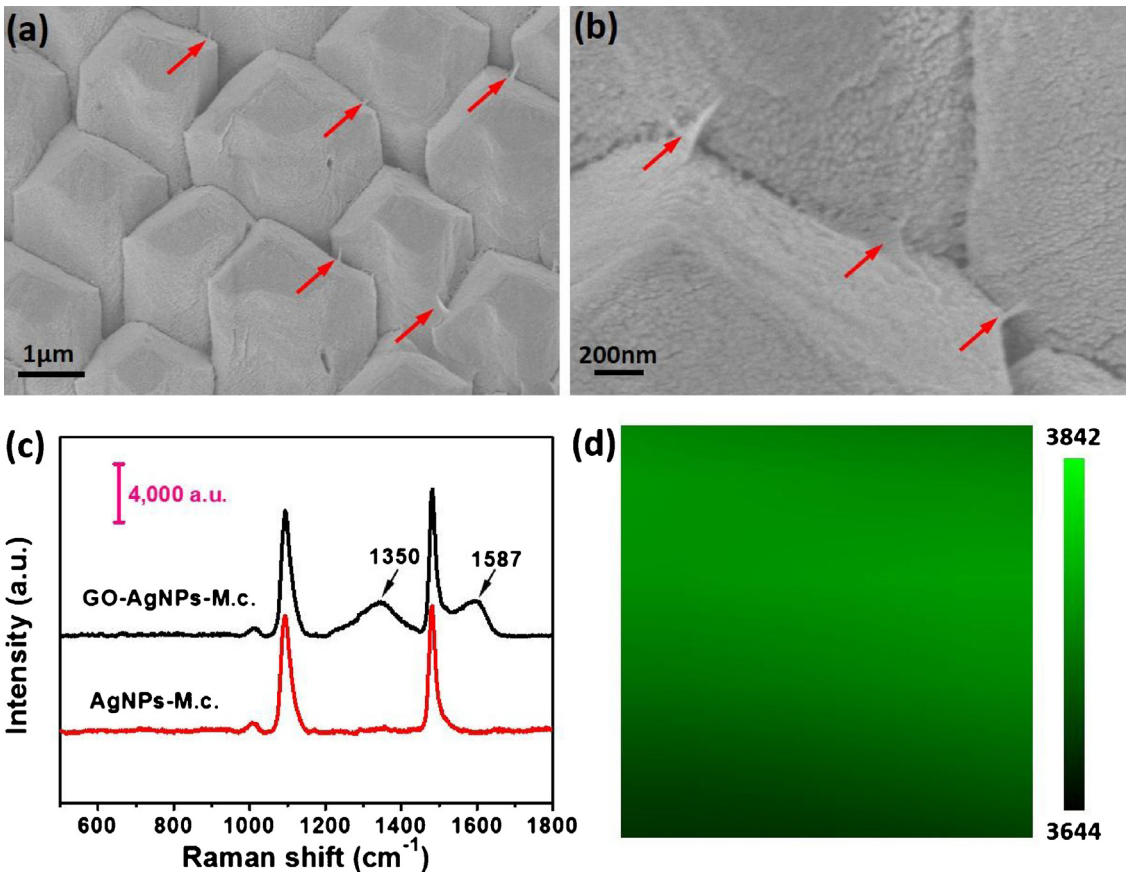

Fig. 4. (a) and (b) are typical SEM images of the FP region on the GO-AgNPs-M.c. substrate in different magnifications. (c) Raman spectra on the GO-AgNPs-M.c. and AgNPs-M.c. substrates. (d) Raman mapping of 1350 cm^{-1} peak of GO on the GO-AgNPs-M.c. substrate over an area of $20 \times 20\ \mu m^2$.

Considering that the GO mainly amplifies the Raman signal via the CM mechanism, and it has little effect on the electric field, so we utilized the COMSOL (RF module) Multiphysics software to simulate the electric field distribution on the AgNPs-M.c. structure. In the simulation, we set the particle size of AgNPs as 20 nm and the gap of the adjacent AgNPs as 3 nm. Fig. 6 shows the x-z view of the local electric field distribution on the AgNPs-M.c. structure that the adjacent prisms are arranged with angle at 90° and 60°, respectively. The relatively intense local electric field is distributed in the narrow space between the adjacent prisms. The electric field enhancement contributed in case of the narrow space with angle at 90° is 10.1-fold, which is slightly lower than the 11.9-fold electric field enhancement provided with the narrow space with angle at 60°. With the angle decreasing, the closer nanoparticles at the bottom of the gap could contribute to the relatively higher electric field enhancement. Thence, by the calculated result, we conclude that the unique natural structure decorated with the dense AgNPs could provide the well electric field enhancement contribution.

As an efficient SERS substrate, aside from the outstanding sensitivity, the high reproducibility is another vital parameter for practical detection. Hence, the SERRS signals of the R6G molecules with the concentration of 10^{-9} M were detected to evaluate the reproducibility of the GO-AgNPs-M.c. substrate. Fig. 7(a) displays the SERRS signals collected from 20 positions randomly within an area of $50 \times 50\ \mu m^2$ on the same GO-AgNPs-M.c. substrate. The profiles of the collected spectra are very similar with the detected position changing. Neither a significant shift of the characteristic Raman bands nor the obvious change of the peak intensity could be observed, showing the well reproducible property of the GO-AgNPs-M.c. substrate. Moreover, as illustrated in Fig. 7(b), the intense SERRS sensitivity at 610 cm^{-1} was quantified and plotted in the form of distribution histogram to analyze the relative standard deviation (RSD) [44]. The black horizontal line represents the average SERRS intensity of 610 cm^{-1} peaks from 20 positions, the shaded area shows the fluctuation of SERRS signals. The RSD of the intensity of the 610 cm^{-1} peak is 6.6% by calculation, further confirming that the GO-AgNPs-M.c. substrate possesses the good reproducibility. The results are attributed to the large-area well-ordered natural arrays and the uniform decoration of GO, making the GO-AgNPs-M.c. substrate act as the reproducible platform for the SERS applications.

For the fabricated GO-AgNPs-M.c. substrate, the GO was likewise introduced as a protective layer to prevent the oxidation of AgNPs. Therefore, the antioxidant stability of the GO-AgNPs-M.c. and AgNPs-M.c. substrates was investigated by the detection of R6G with the concentration of 10^{-9} M. Fig. 8(a) and (b) illustrate the SERRS signals from two substrates under the exposure to the common air environment for 0 day and 15 days, separately. The peak intensity of 610 cm^{-1} was chosen to compare the influence of the aerobic exposure for two substrates. By calculation, the decrease of the peak intensity on the GO-AgNPs-M.c. is only 8.4%. However, the peak intensity of 610 cm^{-1} on the AgNPs-M.c. substrate has the drastic drop i.e. 44.7%, which is assigned to the decrease of the EM caused by the oxidation of AgNPs. In consequence, we can conclude that the GO decoration can endow the GO-AgNPs-M.c. substrate the well antioxidant stability on account of its superior chemical characteristic.

What's more, the feasibility of the GO-AgNPs-M.c. substrate in practical applications was further demonstrated by the detection of malachite green (MG) and methylene blue (MB). As a low-cost and highly efficient fungicide in the aquaculture samples, the high residual MG can cause severe harms to human body in terms of high

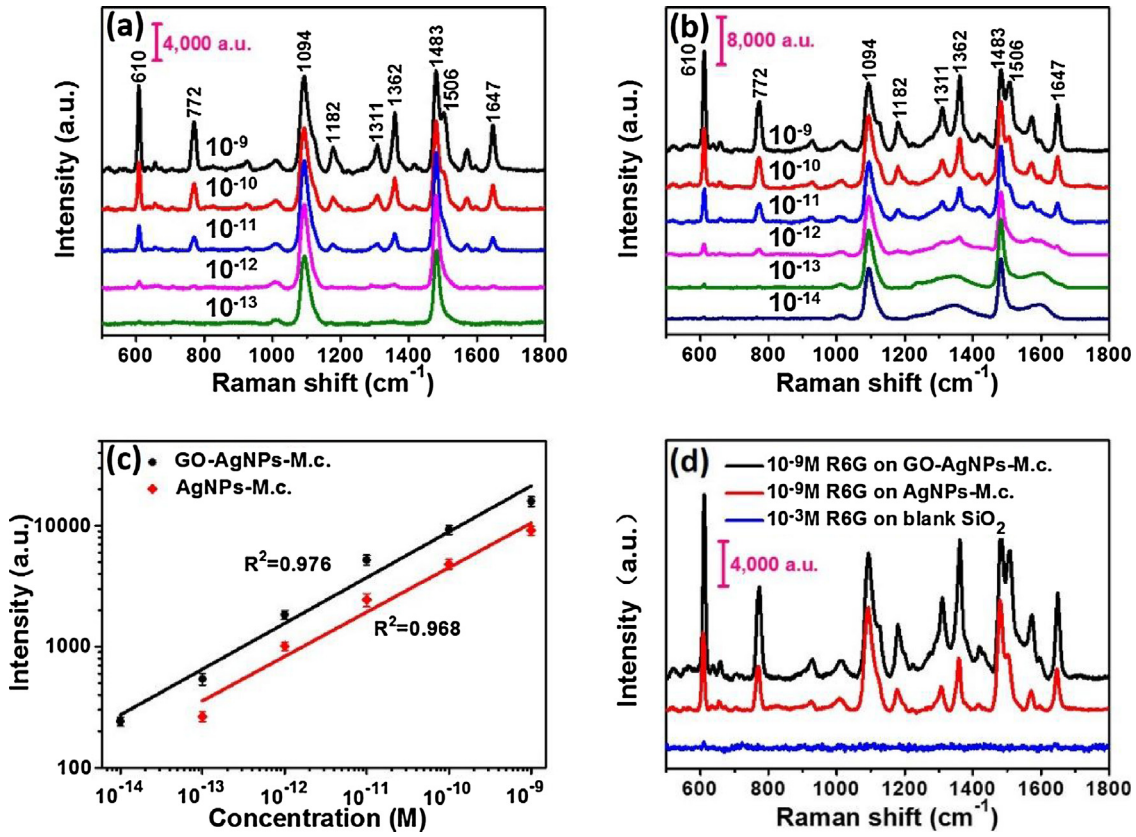

Fig. 5. (a) and (b) are respectively the SERRS signals of R6G molecules with different concentrations on the AgNPs-M.c. and GO-AgNPs-M.c. substrates. (c) Raman intensity of 610 cm^{-1} peaks as a function of different concentrations in log scale on the GO-AgNPs-M.c. and AgNPs-M.c. substrates. (d) SERRS signals of 10^{-9} M R6G on the GO-AgNPs-M.c. and AgNPs-M.c. substrates, the resonance Raman signal of 10^{-3} M R6G on the SiO_2 substrate.

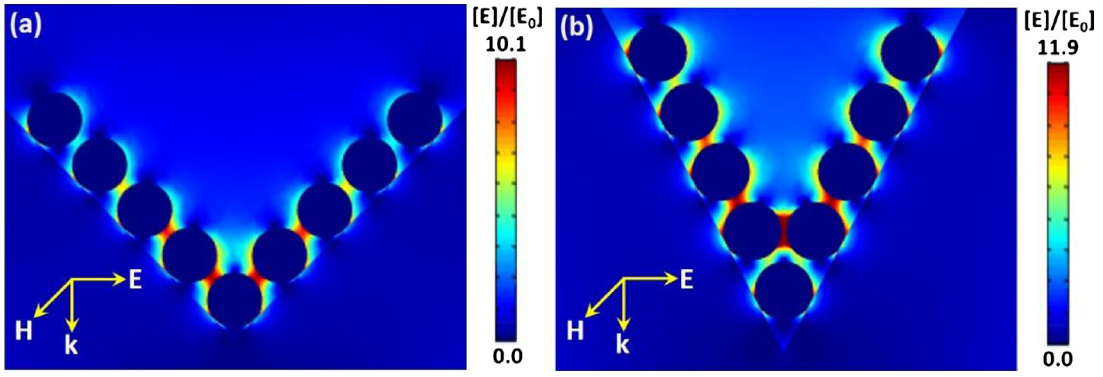

Fig. 6. COMSOL-simulated x-z view of the local electric field distribution on the AgNPs-M.c. structure that the adjacent prisms are arranged with angle at (a) 90° and (b) 60°, respectively. E–electric field; H–magnetic field; k–direction of light propagation.

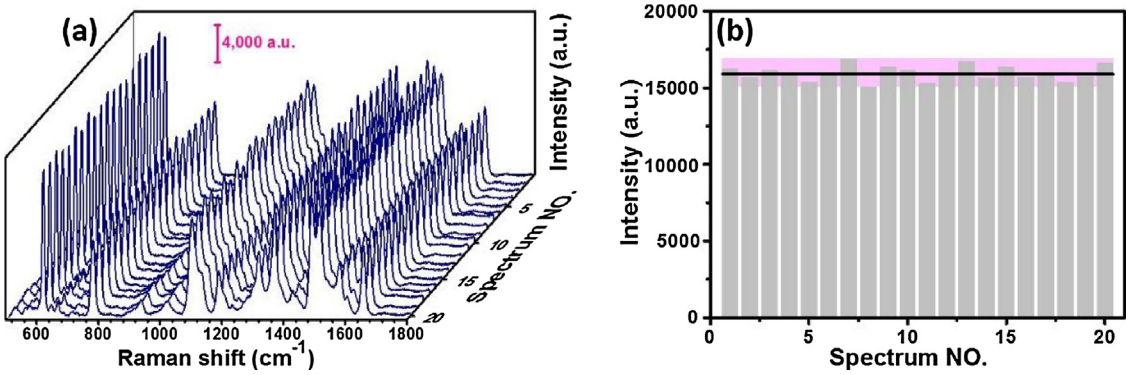

Fig. 7. (a) Collected SERRS signals of R6G with the concentration of 10^{-9} M from 20 randomly selected positions within an area of $50 \times 50\ \mu m^2$ on the GO-AgNPs-M.c. substrate. (b) The intensity variation of 610 cm^{-1} peak for the GO-AgNPs-M.c. substrate.

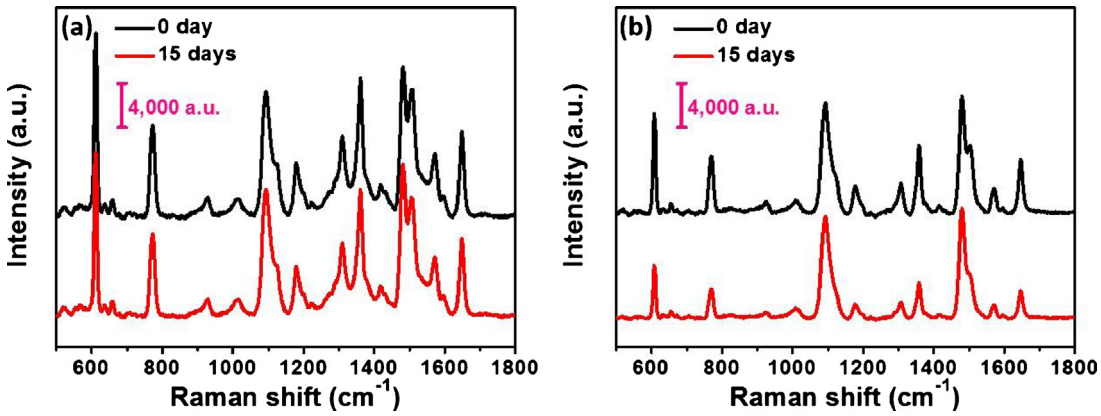

Fig. 8. (a) and (b) are respectively the SERRS signals of R6G with the concentration of 10^{-9} M on the GO-AgNPs-M.c. and AgNPs-M.c. substrates under the exposure to the common air environment for 0 day and 15 days.

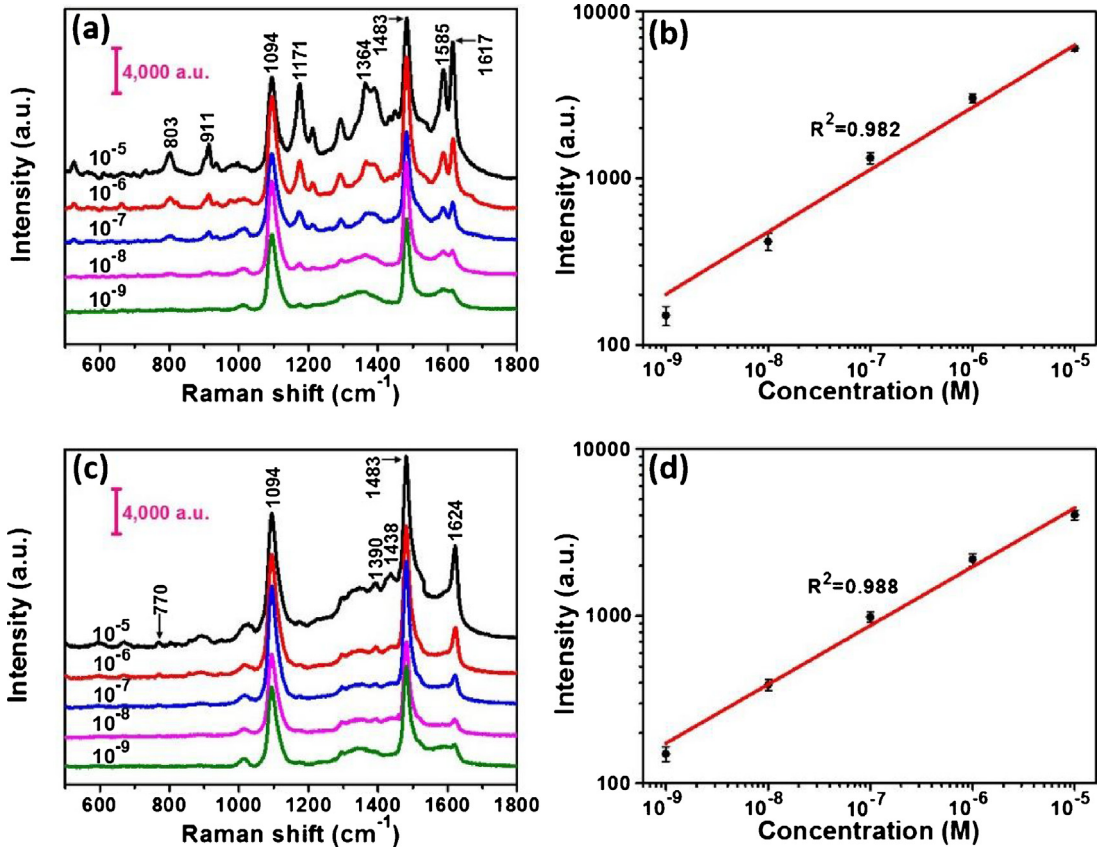

Fig. 9. (a) The SERS spectra of MG with different concentrations on the GO-AgNPs-M.c. substrate. (b) Raman intensity of MG at 1617 cm^{-1} as a function of different concentrations in log scale. (c) The SERS spectra of MB with different concentrations on the GO-AgNPs-M.c. substrate. (d) Raman intensity of MB at 1624 cm^{-1} as a function of different concentrations in log scale.

carcinogenicity, mutagenicity and teratogenicity [45,46]. Hence, the sensitive analysis of trace MG molecules plays a significant role in human health. The SERS spectra of MG with the concentrations range from 10^{-5} to 10^{-9} M were detected on the GO-AgNPs-M.c. substrate. Fig. 9(a) illustrates the dominating characteristic bands of MG in the region from 500 to 1800 cm^{-1}. The primary Raman vibrations of MG are all observed in the spectra. The bands at 803, 911, 1171, 1364 cm^{-1} are related to ring C—H out-of-plane bending, C—H out-of-plane bending and ring skeletal vibration, in-plane vibrations of ring C—H, and N-phenyl stretching vibrations respectively. The peaks located at 1585 and 1617 cm^{-1} are assigned to ring C—C stretching vibration [47]. In addition, the related Raman bands of the CO_3^{2-} ions and the GO could be still observed. The relatively strong SERS peak at 1617 cm^{-1} was chosen to indicate the relationship between the presented SERS intensity and the MG concentration in log scale. The reasonable linear fit curve ($R^2 = 0.982$) in Fig. 9(b) shows the excellent capability for the quantitative detection of MG. Besides, the sensitive detection of MB with the concentrations from 10^{-5} to 10^{-9} M further proves the well practicability of the GO-AgNPs-M.c. substrate. The MB has been reported as one highly toxic dye in various types of aquatic products. Adverse health effects caused by the MB toxicity include skin irritation, convulsions, tachycardia, dyspnea, cyanosis, renal failure, hyperbilirubinemia and hemolytic anemia [48,49]. As shown in Fig. 9(c),

the relatively intense characteristic peaks of MB were obtained in the region from 400 to 1800 cm^{-1}. The relatively intense bands are in-plane bending mode of C—H at 770 cm^{-1}, the symmetric and asymmetric C—N stretches at 1390 and 1438 cm^{-1}, and the ring stretch at 1624 cm^{-1} respectively [50]. As shown in Fig. 9(d), the R^2 of the linear fit calibration curve for the peak at 1624 cm^{-1} can reach 0.988, showing the well capability for the quantitative detection of MB. Therefore, the well sensitive detection of MB and MG show that the GO-AgNPs-M.c. hybrids possess immerse potential for the practical applications in the environmental protection and food security.

4. Conclusion

In summary, we fabricated an efficient natural SERS platform based on the GO-AgNPs-M.c. hybrids with a simply convenient and inexpensive method. With R6G as the analyte molecules, the FP region exhibits the most intriguing SERRS performance compared with other regions, which could be mainly attributed to abundant hot spots existed between mass uniform prisms. More importantly, the GO-AgNPs-M.c. hybrids can achieve highly sensitive SERRS measurements with brilliant reproducibility and antioxidant stability. It has a minimum detectable concentration for R6G as low as 10^{-14} M. The well electric field contribution is confirmed in theory via the COMSOL software. Besides, the GO-AgNPs-M.c. hybrids still obtain the excellent reproducibility with a RSD of 6.6%. The experimental results demonstrate that the covered GO film not only provide an additional enhancement for the SERS signal from CM, but also ensure the stability of the GO-AgNPs-M.c. hybrids from the oxidation. In addition, this novel SERS natural substrate could be still successfully applied in the detection of MG and MB molecules. Therefore, the GO-AgNPs-M.c. substrate, as an effective SERS platform, can pave a new way to facilitate practical SERS applications in diverse biochemical fields.

Acknowledgements

The authors are grateful for financial support from National Natural Science Foundation of China (NSFC) (Grant No. 11504209, 11604040, 11674199 and 11774208) and Excellent Young Scholars Research Fund of Shandong Normal University and Shandong Province Natural Science Foundation (ZR2014FQ032, ZR2017BA004 and 2017GGX20120)

References

[1] S. Nie, S.R. Emory, Probing single molecules and single nanoparticles by surface-enhanced Raman scattering, Science 275 (1997) 1102–1106.
[2] K. Kneipp, Y. Wang, H. Kneipp, L.T. Perelman, I. Itzkan, R.R. Dasari, M.S. Feld, Single molecule detection using surface-enhanced Raman scattering (SERS), Phys. Rev. Lett. 78 (1997) 1667–1670.
[3] Y. Fang, N.H. Seong, D.D. Dlott, Measurement of the distribution of site enhancements in surface-enhanced Raman scattering, Science 321 (2008) 388–392.
[4] A. Barhoumi, N.J. Halas, Label-free detection of DNA hybridization using surface enhanced Raman spectroscopy, J. Am. Chem. Soc. 132 (2010) 12792–12793.
[5] W.E. Doering, M.E. Piotti, M.J. Natan, SERS as a foundation for nanoscale, optically detected biological labels, Adv. Mater. 19 (2007) 3100–3108.
[6] R.M. Jarvis, R. Goodacre, Characterisation and identification of bacteria using SERS, Chem. Soc. Rev. 37 (2008) 931–936.
[7] X.M. Qian, S.M. Nie, Single-molecule and single-nanoparticle SERS: from fundamental mechanisms to biomedical applications, Chem. Soc. Rev. 37 (2008) 912–920.
[8] K.W. Adu, M.D. Williams, M. Reber, R. Jayasingha, H.R. Gutierrez, G.U. Sumanasekera, Probing phonons in nonpolar semiconducting nanowires with Raman spectroscopy, J. Nanotechnol. 2012 (2012) 264198.
[9] J.M. Sylvia, J.A. anni, J.D. Klein, K.M. Spencer, Surface-enhanced Raman detection of 2, 4-dinitrotoluene impurity vapor as a marker to locate landmines, Anal. Chem. 72 (2000) 5834–5840.
[10] A. Campion, P. Kambhampati, Surface-enhanced raman scattering, Chem. Soc. Rev. 27 (1998) 241–250.
[11] J.F. Li, Y.J. Zhang, S.Y. Ding, R. Panneerselvam, Z.Q. Tian, Core-Shell nanoparticle- enhanced Raman spectroscopy, Chem. Rev. 117 (2017) 5002–5069.
[12] H. Xu, J. Aizpurua, M. Kall, P. Apell, Electromagnetic contributions to single-molecule sensitivity in surface-enhanced Raman scattering, Phys. Rev. E 62 (2000) 4318–4324.
[13] S.M. Morton, L. Jensen, Understanding the molecule-surface chemical coupling in SERS, J. Am. Chem. Soc. 131 (2009) 4090–4098.
[14] M. Baia, L. Baia, S. Astilean, J. Popp, Surface-enhanced Raman scattering efficiency of truncated tetrahedral Ag nanoparticle arrays mediated by electromagnetic couplings, Appl. Phys. Lett. 88 (2006) 143121.
[15] K.N. Kanipe, P.P. Chidester, G.D. Stucky, M. Moskovits, Large format surface-enhanced Raman spectroscopy substrate optimized for enhancement and uniformity, ACS Nano 10 (2016) 7566–7571.
[16] J.A. Huang, Y.Q. Zhao, X.J. Zhang, L.F. He, T.L. Wong, Y.S. Chui, S.T. Lee, Ordered Ag/Si nanowires array: wide-range surface-enhanced Raman spectroscopy for reproducible biomolecule detection, Nano Lett. 13 (2013) 5039–5045.
[17] X. Zhang, Z. Dai, S. Si, X. Zhang, W. Wu, H. Deng, C. Jiang, Ultrasensitive SERS substrate integrated with uniform subnanometer scale hot spots created by a graphene spacer for the detection of mercury ions, Small 13 (2017) 160334.
[18] K. Li, Y. Wang, K. Jiang, Y. Ren, Y. Dai, Y. Lu, P. Wang, Large-area, reproducible and sensitive plasmonic MIM substrates for surface-enhanced Raman scattering, Nanotechnology 27 (2016) 495402.
[19] Y. Shin, J. Song, D. Kim, T. Kang, Facile preparation of ultrasmall void metallic nanogap from self-sssembled gold-silica core-shell nanoparticles monolayer via kinetic control, Adv. Mater. 27 (2015) 4344–4350.
[20] C. Zhang, S.Z. Jiang, C. Yang, C.H. Li, Y.Y. Huo, X.Y. Liu, B.Y. Man, Gold@ silver bimetal nanoparticles/pyramidal silicon 3D substrate with high reproducibility for high-performance SERS, Sci. Rep. 6 (2016) 25243.
[21] Z. Li, S.C. Xu, C. Zhang, X.Y. Liu, S.S. Gao, L.T. Hu, H.P. Si, High-performance SERS substrate based on hybrid structure of graphene oxide/AgNPs/Cu film@ pyramid Si, Sci. Rep. 6 (2016) 38539.
[22] C. Zhang, D.A. Mcadams, J.C. Grunlan, Nano/micro-manufacturing of bioinspired materials: a review of methods to mimic natural structures, Adv. Mater. 28 (2016) 6292–6321.
[23] W. Barthlott, M. Mail, B. Bhushan, K. Koch, Plant surfaces: structures and functions for biomimetic innovations, Nano-Micro Lett. 9 (2017) 23.
[24] Z. Mu, X. Zhao, Z. Xie, Y. Zhao, Q. Zhong, L. Bo, Z. Gu, In situ synthesis of gold nanoparticles (AuNPs) in butterfly wings for surface enhanced Raman spectroscopy (SERS), J. Mater. Chem. B 1 (2013) 1607–1613.
[25] S.Y. Chou, C.C. Yu, Y.T. Yen, K.T. Lin, H.L. Chen, W.F. Su, Romantic story or Raman scattering? Rose petals as ecofriendly, low-cost substrates for ultrasensitive surface-enhanced Raman scattering, Anal. Chem. 87 (2015) 6017–6024.
[26] F. Shao, Z. Lu, C. Liu, H. Han, K. Chen, W. Li, J. Chen, Hierarchical nanogaps within bioscaffold arrays as a high-performance SERS substrate for animal virus biosensing, ACS Appl. Mater. Interfaces 6 (2014) 6281–6289.
[27] J.A. Huang, Y.L. Zhang, Y. Zhao, X.L. Zhang, M.L. Sun, W. Zhang, Superhydrophobic SERS chip based on a Ag coated natural taro-leaf, Nanoscale 8 (2016) 11487–11493.
[28] P. Kumar, R. Khosla, M. Soni, D. Deva, S.K. Sharma, A highly sensitive, flexible SERS sensor for malachite green detection based on Ag decorated microstructured PDMS substrate fabricated from Taro leaf as template, Sens. Actuat. B Chem. 246 (2017) 477–486.
[29] Y. Zhu, C. Sun, Y. Song, F. Jiang, X. Yin, M. Tang, H. Ding, The study of the adductor muscle-shell interface structure in three Mollusc species, Acta. Oceanol. Sin. 35 (2016) 57–64.
[30] Y. Song, Y. Lu, H. Ding, H. Lv, G. Gao, C. Sun, Structural characteristics at the adductor muscle and shell interface in mussel, Appl. Biochem. Biotechnol. 171 (2013) 1203–1211.
[31] Z. Liao, L.F. Bao, M.H. Fan, P. Gao, X.X. Wang, C.L. Qin, X.M. Li, In-depth proteomic analysis of nacre, prism, and myostracum of Mytilus shell, J. Proteomics 122 (2015) 26–40.
[32] X. Ling, L. Xie, Y. Fang, H. Xu, H. Zhang, J. Kong, Z. Liu, Can graphene be used as a substrate for Raman enhancement? Nano Lett. 10 (2009) 553–561.
[33] W. Xu, X. Ling, J. Xiao, M.S. Dresselhaus, J. Kong, H. Xu, J. Zhang, Surface enhanced Raman spectroscopy on a flat graphene surface, PANS 109 (2012) 9281–9286.
[34] Y. Wang, Z. Ni, H. Hu, Y. Hao, C.P. Wong, T. Yu, Z.X. Shen, Gold on graphene as a substrate for surface enhanced Raman scattering study, Appl. Phy. Lett. 97 (2010) 163111.
[35] S.C. Xu, S.Z. Jiang, J.H. Wang, J. Wei, W.W. Yue, Y. Ma, Graphene isolated Au nanoparticle arrays with high reproducibility for high-performance surface-enhanced Raman scattering, Sens. Actuat. B Chem. 222 (2016) 1175–1183.
[36] G. Goncalves, P.A. Marques, C.M. Granadeiro, H.I. Nogueira, M.K. Singh, J. Grácio, Surface modification of graphene nanosheets with gold nanoparticles: the role of oxygen moieties at graphene surface on gold nucleation and growth, Chem. Mater. 21 (2009) 4796–4802.
[37] H. Chi, Y.J. Liu, F. Wang, C. He, Highly sensitive and fast response colorimetric humidity sensors based on graphene oxide film, ACS Appl. Mater. Interfaces 7 (2015) 19882–19886.

[38] X. Yu, H. Cai, W. Zhang, X. Li, N. Pan, Y. Luo, X. Wang, J.G. Hou, Tuning chemical enhancement of SERS by controlling the chemical reduction of graphene oxide nanosheets, ACS Nano 5 (2011) 952–958.
[39] C. Zhang, S.Z. Jiang, Y.Y. Huo, A.H. Liu, S.C. Xu, X.Y. Liu, B.Y. Man, SERS detection of R6G based on a novel graphene oxide/silver nanoparticles/silicon pyramid arrays structure, Opt. Express 23 (2015) 24811–24821.
[40] K. Kneipp, Y. Wang, R.R. Dasari, M.S. Feld, Approach to single molecule detection using surface-enhanced resonance Raman scattering (SERRS): a study using Rhodamine 6G on colloidal silver, Appl. Spectrosc. 49 (1995) 780–784.
[41] J. Zhao, O. Chen, D.B. Strasfeld, M.G. Bawendi, Interaction of plasmon and molecular resonances for rhodamine 6G adsorbed on silver nanoparticles, J. Am. Chem. Soc. 129 (2007) 7647–7656.
[42] E.C. Le Ru, E. Blackie, M. Meyer, P.G. Etchegoin, Surface enhanced Raman scattering enhancement factors: a comprehensive study, J. Phys. Chem. C 111 (2007) 13794–13803.
[43] W.B. Cai, B. Ren, X.Q. Li, C.X. She, F.M. Liu, X.W. Cai, Z.Q. Tian, Investigation of surface-enhanced Raman scattering from platinum electrodes using a confocal Raman microscope: dependence of surface roughening pretreatment, Surf. Sci. 406 (1998) 9–22.
[44] J. Zhou, S. Xu, W. Xu, B. Zhao, Y. Ozaki, In situ nucleation and growth of silver nanoparticles in membrane materials: a controllable roughened SERS substrate with high reproducibility, J. Raman Spectrosc. 40 (2009) 31–37.
[45] W. Andersen, S. Turnipseed, J. Roybal, Quantitative confirmatory analyses of malachite green and leucomalachite green residues in fish and shrimp, J. Agric. Food Chem. 54 (2006) 4517–4523.
[46] S.L. Stead, H. Ashwin, B.H. Johnston, A. Dallas, S.A. Kazakov, J.A. Tarbin, M. Sharman, J. Kay, B.J. Keely, An RNA-aptamer-based assay for the detection and analysis of malachite greenand leucomalachite green residues in fish tissue, Anal. Chem. 82 (2010) 2652–2660.
[47] Y. Zhang, K. Lai, J. Zhou, X. Wang, B.A. Rasco, Y. Huang, A novel approach to determine leucomalachite green and malachite green in fish fillets with surface-enhanced Raman spectroscopy (SERS) and multivariate analyses, J. Raman Spectrosc. 43 (2012) 1208–1213.
[48] M. Albert, M.S. Lessin, B.F. Gilchrist, Methylene blue: dangerous dye for neonates, J. Pediatr. Surg. 38 (2003) 1244–1245.
[49] Y.R. Sheynkin, C. Starr, P.S. Li, M. Goldstein, Effect of methylene blue, indigo carmine, and renografin on human sperm motility, Urology 53 (1999) 214–217.
[50] M.S. Akin, M. Yilmaz, E. Babur, B. Ozdemir, H. Erdogan, U. Tamer, G. Demirel, Large area uniform deposition of silver nanoparticles through bio-inspired polydopamine coating on silicon nanowire arrays for practical SERS applications, J. Mater. Chem. B 2 (2014) 4894–4900.

Biographies

Zhengyi Lu is now studying as a master's course student in School of Physics and Electronics, Shandong Normal University, People's Republic of China. His research interests are the synthesis and applications of nanomaterials.

Yanjun Liu is working as a university lecturer in Department of Electrical and Electronic Engineering, Southern University of Science and Technology, People's Republic of China. He received his Ph.D. degree from Nanyang Technological University in 2007. His research interests mainly include surface plasmon polaritons, chiral surface plasmon polaritons, metamaterials and liquid crystal photonics.

Minghong Wang is studying in School of Physics and Electronics, Shandong Normal University, People's Republic of China as a master's course student. Her research interest is the simulation the optical properties of two-dimension materials.

Chao Zhang is working as a researcher in School of Physics and Electronics, Shandong Normal University, People's Republic of China. He received his Ph.D. degree from School of Physics and Electronics, Shandong Normal University in 2016. His research interests include the synthesis and applications of functional materials, such as graphene and Bi_2Se_3.

Zhen Li is a master's and doctorate combined course student in School of Physics and Electronics, Shandong Normal University, People's Republic of China. His research interests are mainly centered on the preparations and applications of MoS_2, WS_2 and graphene.

Yanyan Huo is now working as a university lecturer in School of Physics and Electronics, Shandong Normal University, People's Republic of China. She obtained her Ph.D. degree from State Key Laboratory of Precision Spectroscopy, East China Normal University in 2014. Her research interests are mainly centered on optical properties and applications of metal nanostructures.

Zhe Li is currently studying in School of Physics and Electronics, Shandong Normal University, People's Republic of China as a master's course student. Now he mainly focuses the research interest on the fiber sensor.

Shicai Xu is working as a researcher in the College of Physics and Electronic Information, Dezhou University, People's Republic of China. He received his Ph.D. degree from School of Physics and Electronics, Shandong Normal University in 2014. Currently, he is working on the fields of graphene grown by CVD technology, methods of graphene transferred and DNA nanotechnology

Baoyuan Man is now working as a university lecturer in School of Physics and Electronics, Shandong Normal University, People's Republic of China. He obtained his Ph.D. degree from Department of Optical Engineering, Shandong University. He then joined in Institute of Physics CAS (China) and Trento University (Italy) for postdoctoral research from 1998 to 2002. At present, he researches on the preparation, characterization and application of nanomaterials.

Shouzhen Jiang is currently working as a university lecturer in School of Physics and Electronics, Shandong Normal University, People's Republic of China. He obtained his Ph.D. degree from Shandong University in 2007. Now, his research area is the optical properties of Dirac materials.